

Angular dependence of vertical force and torque when magnetic dipole moves vertically above flat high-temperature superconductor

Yong Yang(杨勇), Shuai-Jie Yang(杨帅杰), Wen-Li Yang(杨文莉), and Yun-Yi Wu(吴云翼)
Citation: Chin. Phys. B, 2021, 30 (**12**): 127401. DOI: 10.1088/1674-1056/ac0697
Journal homepage: http://cpb.iphy.ac.cn; http://iopscience.iop.org/cpb

What follows is a list of articles you may be interested in

Lateral magnetic stiffness under different parameters in a high-temperature superconductor levitation system

Yong Yang(杨勇) and Yun-Yi Wu(吴云翼)
Chin. Phys. B, 2021, 30 (**7**): 077404. DOI: 10.1088/1674-1056/abe0c2

NMR and NQR studies on transition-metal arsenide superconductors $LaRu_2As_2$, $KCa_2Fe_4As_4F_2$, and $A_2Cr_3As_3$

Jun Luo(罗军), Chunguang Wang(王春光) Zhicheng Wang(王志成), Qi Guo(郭琦), Jie Yang(杨杰), Rui Zhou(周睿), K Matano, T Oguchi, Zhian Ren(任治安), Guanghan Cao(曹光旱), Guo-Qing Zheng(郑国庆)
Chin. Phys. B, 2020, 29 (**6**): 067402. DOI: 10.1088/1674-1056/ab892d

Electrochemical synthesis of alkali-intercalated iron selenide superconductors

Shen Shi-Jie, Ying Tian-Ping, Wang Gang, Jin Shi-Feng, Zhang Han, Lin Zhi-Ping, Chen Xiao-Long
Chin. Phys. B, 2015, 24 (**11**): 117406. DOI: 10.1088/1674-1056/24/11/117406

Optimization of intergrain connection in high-temperature superconductor $Bi_2Sr_2CaCu_2O_x$

Li Cheng-Shan, Zhang Sheng-Nan, Hao Qing-Bin, Ma Xiao-Bo, Lu Tian-Ni, Zhang Ping-Xiang
Chin. Phys. B, 2015, 24 (**7**): 077401. DOI: 10.1088/1674-1056/24/7/077401

Crystal chemistry and structural design of iron-based superconductors

Jiang Hao, Sun Yun-Lei, Xu Zhu-An, Cao Guang-Han
Chin. Phys. B, 2013, 22 (**8**): 087410. DOI: 10.1088/1674-1056/22/8/087410

Angular dependence of vertical force and torque when magnetic dipole moves vertically above flat high-temperature superconductor*

Yong Yang(杨勇)[1,2,†], Shuai-Jie Yang(杨帅杰)[1], Wen-Li Yang(杨文莉)[1], and Yun-Yi Wu(吴云翼)[3,4]

[1] School of Mechano-Electronic Engineering, Xidian University, Xi'an 710071, China
[2] Shaanxi Key Laboratory of Space Extreme Detection, Xi'an 710071, China
[3] China Three Gorges Science and Technology Research Institute, Beijing 100036, China
[4] Physikalisches Institut B, RWTH Aachen, Aachen 52056, Germany

(Received 10 March 2021; revised manuscript received 16 April 2021; accepted manuscript online 29 May 2021)

The interaction between a permanent magnet (PM) assumed as a magnetic dipole and a flat high-temperature superconductor (HTS) is calculated by the advanced frozen-image model. When the dipole vertically moves above the semi-infinite HTS, the general analytical expression of vertical force and that of torque are obtained for an arbitrary angle between the magnetization direction of the PM and the *c* axis of the HTS. The variations of the force and torque are analyzed for angle and vertical movements in both zero-field cooling (ZFC) condition and field cooling (FC) condition. It is found that the maximum vertical repulsive or attractive force has the positive or negative cosine relation with the angle. However, the maximum torque has the positive or negative sine relation. From the viewpoint of the rotational equilibrium, the orientation of the magnetic dipole with zero angle is deemed to be an unstable equilibrium point in ZFC, but the same orientation is considered as a stable equilibrium point in FC. In addition, both of the variation cycles of the maximum force and torque with the angle are π.

Keywords: high-temperature superconductor, magnetic dipole, frozen-image model, angle

PACS: 74.72.–h, 84.71.Ba, 85.25.Am, 85.70.Rp **DOI:** 10.1088/1674-1056/ac0697

1. Introduction

The passive levitation between bulk high-temperature superconductors (HTSs) and permanent magnets (PMs) can simultaneously provide the stability in different directions due to the strong flux pinning characteristic of HTS. Since the discovery of HTS in 1986, the HTS levitation has been successfully applied to many practical engineering aspects, such as the superconducting magnetic levitation vehicles[1–3] and the bearings for flywheel energy storage system.[4–6] At the same time, a large number of studies have been performed to improve the levitation performances including vertical force, lateral force, magnetic stiffness, *etc*.[7–13] In addition, it has been found experimentally that the angle between the magnetization direction of the PM and the *c* axis of the HTS significantly affects the levitation properties.[14–18] In fact, the magnetization direction of the PM does not often coincide with the *c* axis of the HTS in many practical applications.

More than 20 years ago, Shi *et al.*[14] and Tent *et al.*[15] experimentally investigated that the domain orientation affects the levitation force for the cubic and spherical geometries of the HTS samples, respectively. They found that the levitation force varies in a cosine law fashion with the angle between the direction of the magnetic field and the *c* axis of the HTS. Also, Yang *et al.* measured the levitation forces of the YBCO bulk samples with different grain-orientations at liquid nitrogen temperature.[16,17] It is found that the levitation force decreases monotonically with the angle between the *c* axis and the normal to the polished surface. A simple formula was proposed to describe the relationship between the levitation force and the angle for a relatively low external magnetic field produced by a PM.[17] Very recently, the effect of magnetization angle on the levitation force of the bulk HTS was studied in high magnetic field produced by a superconducting magnet.[18] It was also shown that the levitation force decreases with increasing angle between the upper surface of the bulk HTS and the horizontal plane. In addition, the experimental results[18] indicated that the relationship between the angle and the levitation force of the bulk HTS is complex and cannot be expressed by using Yang's formula[17] in high magnetic field.

In the studies of modelling superconducting magnetic levitation, many different numerical and analytical approaches, such as the models of solving differential Maxwell equations combining different relations between the electric field and the current density in superconductor,[19–25] the method based on the minimization of the magnetic energy[26,27] and the models based on the calculation of magnetic moments,[28–37] have been proposed. A very complete and comprehensive compilation for modelling magnetic levitation can be found in a recent review paper.[38] In the afore-

*Projects supported by the National Natural Science Foundation of China (Grant No. 11572232) and the China Three Gorges Corporation Research Project (Grant No. 202103407).

†Corresponding author. E-mail: yangyong@xidian.edu.cn

© 2021 Chinese Physical Society and IOP Publishing Ltd

mentioned calculation models, the image models of the magnetic diploe have been widely used to design and optimize the superconducting magnetic levitation systems because the models can give the simple and analytical expressions of force, torque, and stiffness and need a very shorter calculation time than the complicated numerical simulation models, such as the finite element method combining the critical state models. The simplest form of the magnetic image model was used to calculate and describe the levitation behavior for a magnetic dipole over a semi-infinite superconducting plane in the Meissner state.[30,31] In this case, the magnetic dipole has only one image named the diamagnetic mirror image below the superconductor top surface. The lateral position of the diamagnetic mirror image is the same as that of the magnetic dipole, and the vertical height below the superconductor surface equals the height of the magnetic dipole above the surface. The simplest form of the image model can describe only the HTS magnetic levitation properties in the zero field cooling (ZFC) case. Kordyuk[32] added a frozen image, which creates the same magnetic field distribution outside the superconductor as the frozen magnetic flux, into the image model to study the field cooling (FC) state of the bulk HTS. Then Hull and Cansiz[33] used the frozen-image model to calculate the vertical force, lateral force, and stiffness, and found the calculations to be in good agreement with their measurements when they used the equivalent current loops in the axisymmetric case to calculate the vertical force. But the frozen-image model did not predict hysteresis in the vertical force or lateral force and could not give the lateral force in ZFC either, because the frozen-image model did not take into account the flux flow as the PM moved. To remedy these problems, Yang and Zheng have proposed introducing two additional magnetic dipoles they called the vertical and horizontal movement images respectively, to consider the magnetic flux changes due to the vertical and lateral motions of the PM.[34] Subsequently Zhang *et al.* amended the location of the vertical movement image below the HTS surface to obtain the relationship between the maximum levitation forces and the initial cooling heights.[35] In addition, Wu *et al.*[36] modified the change rules of the vertical movement image in the advanced frozen-image model proposed by Yang and Zheng[34] to describe the hysteresis loops in the second and subsequent descent–ascent cycles of the PM.

The above theoretical investigations using the magnetic image models do not contain the influence of the angle between the magnetization direction of the PM and the c axis of the bulk HTS on the levitation behavior. The angular dependence of forces has been calculated using the dipole–dipole image model between a small PM and a superconductor in the Meissner state.[39–45] The results showed that the levitation force is maximum when the magnetic moment is perpendicular to the surface and minimum when it is parallel,[39] which is at least in a qualitative agreement with the measured data.[17] Coffey studied the levitation force between a magnetic dipole and a superconducting sphere in the perfect flux exclusion state for two different orientations of the dipole, vertically and horizontally.[40,41] The magnetic force and torque on a superconducting sphere in an arbitrary orientation of the magnetic dipole also were calculated in the Meissner state.[42–45] In addition, the frozen-image model has also been employed to calculate the interaction between a small magnet and an HTS in FC for an arbitrary orientation of the dipole. Alqadi *et al.* analyzed the angular dependence of the levitation force and energy by utilizing the frozen-image model for a system composed of a small magnet and a superconducting sphere.[46] Using the same model, Sivrioglu and Cinar,[47] Sivrioglu and Basaran,[48] and Basaran and Sivrioglu[49] studied the magnetic potentials and stiffness values for the practical ring-shaped PM–HTS bearings with the variation of the angle between the rotational magnetization symmetry axis of the PM and the levitation direction. Although the interaction between the PM and the HTS with angle has been studied by using the image or frozen-image model in the literature, the angular dependence of force and torque has not yet been investigated so far by utilizing the advanced frozen-image model, which can consider the flux change due to the motion of the PM. Moreover, the torque between a superconductor and a magnet has been seldom studied and was reported only for the Meissner state.[44,45]

In this paper, the PM–HTS levitation system is simplified into a magnetic dipole levitated above the semi-infinite flat HTS. Based on the magnetic field distribution of the magnetic dipole directing to an arbitrary direction, the levitation force and torque on the PM are calculated by using the advanced frozen-image model with an arbitrary angle between the magnetization direction of the PM and the c axis of the semi-infinite flat HTS. The variations of the levitation force and torque with the angle are obtained as the PM moves vertically above the HTS. The rest of this paper is structured as follows. In Section 2, we describe the advanced frozen-image model for the vertical motions of the PM with arbitrary angle in the ZFC condition and the FC condition, and derive the generally analytical expressions of the magnetic field, force and torque. In Section 3, the results of the levitation force and torque under different angles are presented and discussed in the ZFC condition and the FC condition as the PM moves vertically. Finally, the conclusions are drawn in Section 4.

2. Calculation model for force and torque

Figure 1 shows a schematic diagram of the calculation model. The PM is simplified as a magnetic dipole with the magnetic moment $\boldsymbol{m}_1$, has an angle θ with respect to the z

axis. The bulk HTS is assumed to have a semi-infinite structure. The origin of rectangular Cartesian coordinate system is taken at the center of the bulk HTS surface. Based on the magnetic image method in the electrodynamics and the advanced frozen-image model,[34] the diamagnetic image $\boldsymbol{m}_2$ having an angle of π–θ moves as the PM moves. The frozen image $\boldsymbol{m}_3$ having an angle of $-\theta$ does not moves and has a fixed position below the HTS surface. The vertical movement image $\boldsymbol{m}_4$ having an angle of π–θ in ZFC or an angle of $-\theta$ in FC also has a fixed position. According to previous studies,[33,34] the vector moduli of $\boldsymbol{m}_1$, $\boldsymbol{m}_2$, and $\boldsymbol{m}_3$ have the same value, however, the modulus of $\boldsymbol{m}_4$ changes as the PM vertically moves. The images of $\boldsymbol{m}_3$ and $\boldsymbol{m}_4$ have the stationary positions $(0,-h)$ and $(0,-z_0)$, respectively, where h is the initial cooling height and z_0 is the minimum vertical gap between the PM and the HTS surface. The image of $\boldsymbol{m}_2$ has a changing position $(0,-z)$ as the PM vertically moves.

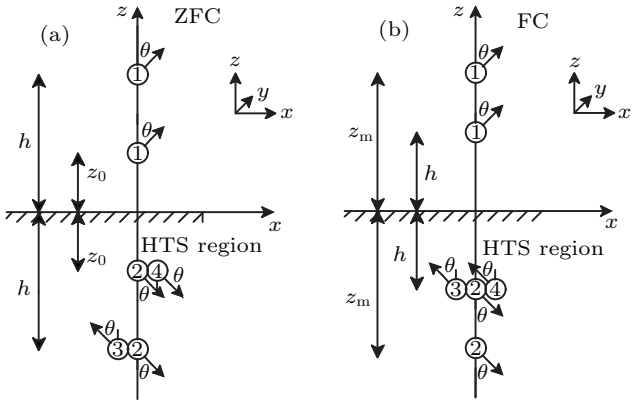


Fig. 1. Schematic diagram of advanced frozen-image model with arbitrary angle θ between the magnetization direction of the PM and the c axis of the HTS under (a) ZFC and (b) FC, with 1–4 representing PM, diamagnetic image, frozen image, and vertical movement image, respectively, h being initial cooling height, z_0 and $z_{\rm m}$ denoting minimum and maximum vertical gaps between the PM and the HTS surfaces, respectively, h bing equal to z_0 in FC.

From magnetomechanics, the force and torque between two magnetic dipoles can be given as

$$\boldsymbol{F} = (\boldsymbol{m}\cdot\nabla)\,\boldsymbol{B}, \tag{1}$$

$$\boldsymbol{T} = \boldsymbol{m}\times\boldsymbol{B}, \tag{2}$$

where $\boldsymbol{m}$ refers to the magnetic moment of one dipole, $\boldsymbol{B}$ denotes the magnetic field from the other dipole, and $\boldsymbol{F}$ and $\boldsymbol{T}$ are the force and torque vectors, respectively.

The magnetic field produced by a magnetic dipole having an angle θ with respect to the z axis can be derived from the Biot–Savart's law and the superposition principle. As shown in Fig. 2, the dipole with the magnetic moment $\boldsymbol{m}$ can be considered as a small current loop with radius R and current I. The magnetic moment $\boldsymbol{m}$ of the dipole with θ is decomposed into m_z in the z-axis direction and m_x in the x-axis direction. Using the Biot–Savart's law, the expressions of the magnetic field at any location point $M(x,y,z)$ produced by the vertical component m_z and the lateral component m_x of the magnetic dipole can be obtained as follows:

$$\begin{aligned}
B_{zx} &= \frac{\mu_0 m_z}{4\pi}\frac{3xz}{(x^2+y^2+z^2)^{5/2}},\\
B_{zy} &= \frac{\mu_0 m_z}{4\pi}\frac{3yz}{(x^2+y^2+z^2)^{5/2}},\\
B_{zz} &= \frac{\mu_0 m_z}{4\pi}\frac{2z^2-x^2-y^2}{(x^2+y^2+z^2)^{5/2}},
\end{aligned} \tag{3}$$

$$\begin{aligned}
B_{xx} &= \frac{\mu_0 m_x}{4\pi}\frac{2x^2-z^2-y^2}{(x^2+y^2+z^2)^{5/2}},\\
B_{xy} &= \frac{\mu_0 m_x}{4\pi}\frac{3xy}{(x^2+y^2+z^2)^{5/2}},\\
B_{xz} &= \frac{\mu_0 m_x}{4\pi}\frac{3xz}{(x^2+y^2+z^2)^{5/2}},
\end{aligned} \tag{4}$$

where μ_0 is the permeability of vacuum, the first subscript and the second subscript of the magnetic field components indicate the component of the magnetic moment and the direction of the magnetic field, respectively. Each component of the total magnetic field can be obtained by the superposition of the corresponding components in Eqs. (3) and (4). Therefore, the expressions of the total magnetic field can be given as

$$\begin{aligned}
B_x &= B_{zx}+B_{xx},\\
B_y &= B_{zy}+B_{xy},\\
B_z &= B_{zz}+B_{xz}.
\end{aligned} \tag{5}$$

When the PM moves only vertically along the z-axis direction, according to the superposition principle and Eqs. (1) and (2), the forces and torques acting on the magnetic dipole $\boldsymbol{m}_1$ at coordinate $(0,z)$ due to the diamagnetic dipole $\boldsymbol{m}_2$ at $(0,-z)$, the frozen dipole $\boldsymbol{m}_3$ at $(0,-h)$ and the vertical movement dipole $\boldsymbol{m}_4$ at $(0,-z_0)$ are

$$\begin{aligned}
F_x &= F_y = 0,\\
F_z &= \frac{3\mu_0 m_1(3+\cos 2\theta)}{8\pi}\\
&\quad\times\left(\frac{m_2}{(2z)^4}-\frac{m_3}{(z+h)^4}-\frac{m_4}{(z+z_0)^4}\right),
\end{aligned} \tag{6}$$

$$\begin{aligned}
T_x &= T_z = 0,\\
T_y &= \frac{\mu_0 m_1 \sin 2\theta}{8\pi}\left(\frac{m_2}{(2z)^3}-\frac{m_3}{(z+h)^3}-\frac{m_4}{(z+z_0)^3}\right),
\end{aligned} \tag{7}$$

where m_1, m_2, m_3, and m_4 are the vector modulus of $\boldsymbol{m}_1$, $\boldsymbol{m}_2$, $\boldsymbol{m}_3$, and $\boldsymbol{m}_4$, respectively. From Eqs. (6) and (7), the interactions between the PM with angle θ and the HTS include not only the levitation force F_z, but also the torque T_y, which is distinguished from the interaction between the PM without angle and the HTS. In the practical applications of the HTS levitation systems, the levitation body usually undergoes some disturbances, which may make the body tilt. The torque T_y emerges according to Eq. (7) because the angle θ is not equal to zero. The torque can make the levitation body rotate about

the y axis and determines the rotation stability of the levitation body.

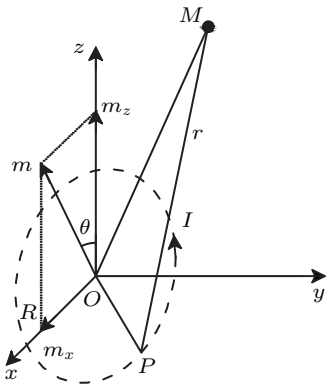


Fig. 2. Schematic diagram for calculating magnetic field at any location point $M(x,y,z)$ produced by dipole with magnetic moment $\boldsymbol{m}$ having angle θ with respect to the z axis, dipole being considered as a small current loop (the dotted circle) with radius R and current I, and m_x and m_z denoting components of $\boldsymbol{m}$ along the x and z directions, respectively.

3. Results and discussion

In the study, the variation rule of m_4 is the same as that in the advanced frozen-image model.[34] We adopt the following parameters: $m_1 = m_2 = m_3 = 5.0 \times 10^{-3}$ A·m^2, $z_0 = 0.5$ mm, $a_1 = 0.1$ A·m, $a_2 = 5.0$ A·m, $b_1 = 5.0 \times 10^{-2}$ A·m, and $b_2 = 0.15$ A·m, where a_1, a_2, b_1, and b_2 are the proportional constants of m_4 for different initial cooling conditions and different vertical movement processes of the PM. The values of initial cooling height h are taken as 30 mm in ZFC and 0.5 mm in FC, respectively. The values of above parameters are identical to those counterparts in a previous paper[34] in order to compare the calculation results with the published ones.

3.1. ZFC case

As the PM firstly descends from the initial cooling position $z = h = 30$ mm to the lowest position $z = z_0$, the direction of the vertical movement image ($\boldsymbol{m}_4$) keeps the same as that of the diamagnetic image ($\boldsymbol{m}_2$) in ZFC because the magnetization of the bulk HTS is diamagnetic (Fig. 1(a)). In the PM descending and ascending processes, the values of the vertical movement image can be obtained by the rules of $\boldsymbol{m}_4$ under ZFC through using the proportional constants of a_1 and a_2 in the advanced frozen-image model.[34] Figure 3 shows the curves of typical levitation force with different angles in ZFC. At each vertical gap, the repulsive vertical force generally decreases as the angle increases from 0 to $\pi/2$, which qualitatively accord with the curves of measured levitation force with different values of θ.[17] Moreover, the area of the hysteresis cycle also decreases with θ increasing. As the angle of the PM increases, the magnetic field that the bulk HTS feels may decrease though the relative location of the PM never changes. This leads to the fact that the levitation force and the area of the hysteresis cycle decrease. The inset of Fig. 3 displays the effect of θ on the maximum value of the levitation force. It is obvious that the maximum vertical repulsive force changes as a cosine law fashion when the angle increases from 0 to 2π, which is also in agreement with the experimental result reported by Tent *et al.*[15] The cycle of the cosine law is π. Although the calculation results of vertical force in the present paper are consistent qualitatively with the previous experimental data,[15,17] the advanced frozen-image model with arbitrary angle θ cannot give the quantitative calculations either, because the model does not contain the size effect of the HTS levitation system. However, the model should give the quantitative results including the size effect of the superconducting levitation system if the PM and its images are replaced by Amperian current loops.

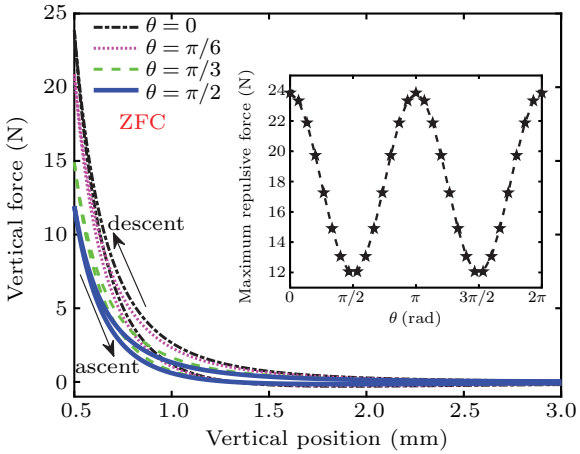


Fig. 3. Curves of levitation force *versus* levitation height at different angles $\theta = 0$, $\pi/6$, $\pi/3$, and $\pi/2$ in ZFC, with inset showing relationship between maximum vertical repulsive force and angle changing from 0 to 2π.

Figure 4 shows the variations of torque T_y with vertical height at different angles in ZFC when the PM vertically descends and ascends. The torque on the PM appears if the angle is not equal to zero and increases as the angle increases from 0 to $\pi/4$. The magnetic hysteresis effect can also be found from the curve of the torque *versus* vertical gap according to the calculations. The torque T_y decreases as the vertical gap between the PM and the HTS increases. The maximum value of T_y is gained at the lowest position for any value of θ. The inset of Fig. 4 displays that the maximum value of T_y varies with angle θ from 0 to 2π. As can be seen from Fig. 4 and its inset, the value of T_y is positive as θ changes from 0 to $\pi/2$ in ZFC. The torque T_y with the positive value tends to align the PM parallelly to the HTS surface if the orientation of the PM magnetization deviates from the z axis. From the viewpoint of the rotational equilibrium, $\theta = 0$ is thereby deemed to be an unstable equilibrium point in ZFC, which accords with the result of the torque between a superconductor sphere in the Meissner state and a finite-size PM reported by Diez–Jimenez

et al.[45] The maximum T_y changes as a sine law fashion when the angle increases from 0 to 2π, which means that the characteristic of the θ-dependent T_y is different from that of the θ-dependent levitation force for the same cooling condition. The cycle of the sine law is π. At any vertical position, the torque is maximum at $\theta = \pi/4 + n\pi/2$, where n is any arbitrary integer. In addition, the toque T_y is equal to zero as the magnetization direction of the PM is perpendicular or parallel to the a–b plane of the HTS bulk.

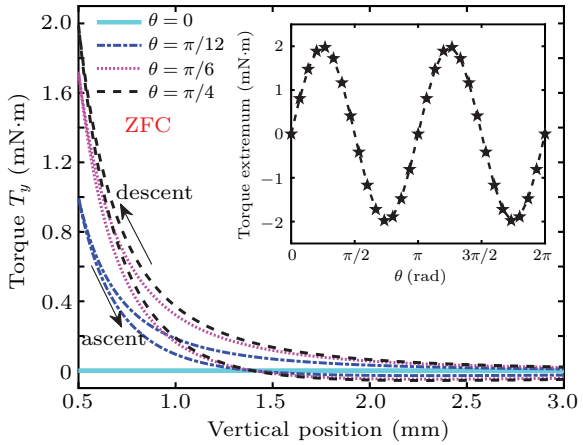


Fig. 4. Variations of torque T_y with levitation height at different angles $\theta = 0$, $\pi/12$, $\pi/6$, and $\pi/4$ in ZFC, with inset showing relationship between maximum torque and angle varying from 0 to 2π.

3.2. FC case

When the PM ascends from the initial cooling position $z = h$ to the highest position $z = z_m$, the orientation of $\boldsymbol{m}_4$ is considered as that of the frozen image $\boldsymbol{m}_3$ in FC because the magnetization of the bulk HTS is paramagnetic (Fig. 1(b)). The values of the vertical movement image can be obtained by the rules of $\boldsymbol{m}_4$ under FC using the proportional constants of b_1 and b_2 in the advanced frozen-image model.[34] Figure 5 shows the relationship between the vertical force and the vertical height at different angles in FC. At each vertical position, no matter whether the process of the PM is ascent or descent, the attractive or repulsive force generally decreases as the angle increases from 0 to $\pi/2$. In addition, the magnetic hysteresis effect is always remarkable for different values of θ, which may be caused by a large quantity of the frozen fluxes in FC. The inset of Fig. 5 displays the θ-dependent maximum vertical repulsive and attractive forces. It is obvious that the maximum repulsive force changes in a cosine law fashion when the angle increases from 0 to 2π. However, the maximum attractive force varies with a negative cosine function because of the negative sign of the attractive force. Like the case in ZFC, the cycle of the positive cosine law and the negative cosine law are also π.

It should be pointed out that the curves of vertical force with $\theta = 0$ in Figs. 3 and 5 are identical to the corresponding curves in Fig. 3 of Ref. [34] because all parameters are identical, which also attests to the calculations credible. Because the calculation results in the present paper are qualitative, the reliability of the calculations cannot be confirmed by quantitatively comparing with the experimental data. But our calculations qualitatively accord with the experimental[15,17,33] and theoretical[34,45] results.

Comparing Fig. 3 with Fig. 5, one can find that the maximum vertical repulsive force in ZFC is much larger than that in FC under the same angle. The reason is that the maximum vertical repulsive force is determined by the diamagnetic property of the HTS for a certain levitation system. In the ZFC, the HTS is dominated primarily by the diamagnetic property, while in the FC, the HTS is governed mainly by the flux pinning characteristic. Therefore, the levitation force usually appears much bigger in the ZFC than in the FC. Previous experimental results[33] with $\theta = 0$ also showed such a characteristic of the vertical force in different cooling conditions.

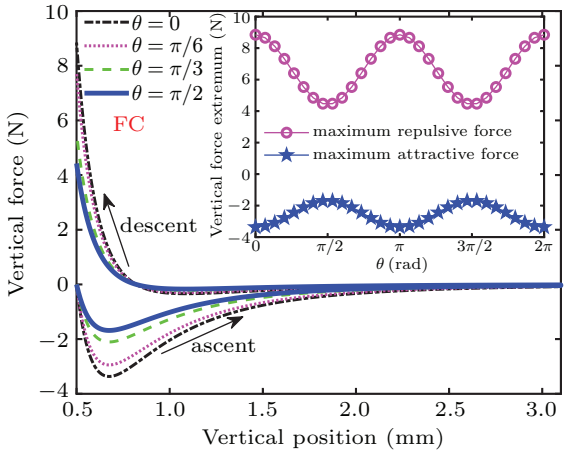


Fig. 5. Curves of vertical force *versus* vertical height at different angles $\theta = 0$, $\pi/6$, $\pi/3$, and $\pi/2$ in FC, with inset showing angular dependence of the maximum vertical repulsive and attractive forces.

Figure 6 shows the variations of the torque T_y with vertical height at different angles in FC when the PM vertically ascends and descends. At each vertical position, the absolute value of T_y generally increases as the angle increases from 0 to $\pi/4$. The inset of Fig. 6 displays that the extreme value of T_y changes with angle θ from 0 to 2π in FC. From Fig. 6 and its inset, it follows that the torque on the PM has a negative value during ascent in FC as the angle varies from 0 to $\pi/2$. The torque T_y with the negative value tends to rotate the PM to its original orientation if the direction of the PM magnetization deviates from the z axis. Therefore, $\theta = 0$ is considered as a stable equilibrium point during ascent in the FC, which is distinguished from the unstable equilibrium point at the same angle in the ZFC. But the torque T_y has positive value during descent at a small vertical gap because the diamagnetic property of the HTS is enhanced as the PM approaches to the HTS.

The extreme value of T_y changes as a negative sine law fashion during ascent when the angle increases from 0 to 2π, however, the torque extremum varies with a positive sine function during descent. The cycle of the negative sine law and positive sine law are both π. Like the case in ZFC, at any vertical position, the torque obtains the extreme values at $\theta = \pi/4 + n\pi/2$.

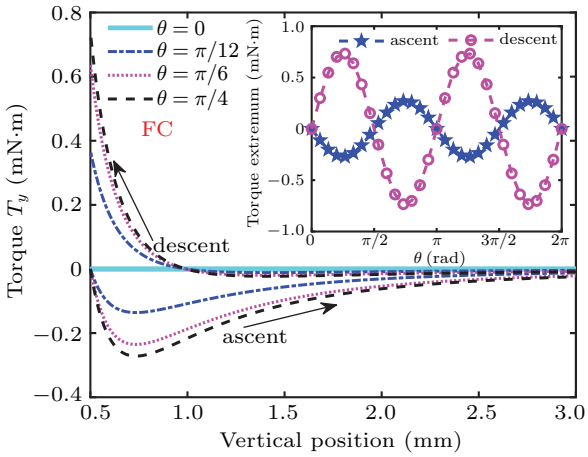


Fig. 6. Variations of torque T_y with levitation height at different angles $\theta = 0$, $\pi/12$, $\pi/6$, and $\pi/4$ in FC, with inset showing angular dependence of torque extremum.

4. Conclusions

The vertical force F_z and rotational torque T_y are calculated by the advanced frozen-image model[34] when the PM vertically moves above the semi-infinite HTS. The PM has an angle θ with respect to the c axis of the HTS. The torque T_y appears due to the non-zero θ. Different results of the levitation force F_z and torque T_y for the ZFC condition and the FC condition are summarized as follows.

(i) For both cooling conditions, the repulsive or attractive vertical force decreases with θ increasing from 0 to $\pi/2$.

(ii) When increasing θ, the maximum repulsive vertical force changes as a positive cosine law fashion in ZFC and FC, however the maximum attractive force varies with a negative cosine law in FC.

(iii) For both cooling conditions, the absolute value of T_y generally increases with θ increasing from 0 to $\pi/4$.

(iv) From the viewpoint of the rotational equilibrium, $\theta = 0$ is thereby deemed to be an unstable equilibrium point in ZFC, however, $\theta = 0$ is considered as a stable equilibrium point in FC.

References

[1] Wang J, Wang S, Zeng Y, *et al.* 2002 *Physica C* 378–381, Part 1 809
[2] Mattos L S, Rodriguez E, Costa F, Sotelo G G, de Andrade R and Stephan R M 2016 *IEEE Trans. Appl. Supercond.* **26** 3600704
[3] Hong W, Xin Y, Wang C, Wen Y, Zhao C and Li W 2020 *IEEE Trans. Appl. Supercond.* **30** 3603210
[4] Werfel F N, Floegel-Delor U, Rothfeld R, Riedel T, Goebel B, Wippich D and Schirrmeister P 2012 *Supercond. Sci. Technol.* **25** 014007
[5] Miyazaki Y, Mizuno K, Yamashita T, Ogata M, Hasegawa H, Nagashima K, Mukoyama S, Matsuoka T, Nakao K, Horiuch S, Maeda T and Shimizu H 2016 *Cryogenics* **80** 234
[6] Espenhahn T, Wunderwald F, Möller M, Sparing M, Hossain M, Fuchs G, Abdkader A, Cherif C, Nielsch K and Hühne R 2020 *J. Phys. D: Appl. Phys.* **53** 035002
[7] Ozturk K, Kabaer M, Abdioglu M, Patel A and Cansiz A 2016 *J. Alloys Compd.* **689** 1076
[8] Ai L, Zhang G, Li W, Liu G and Liu Q 2018 *Physica C* **550** 57
[9] Yang W, Liao D, Ji Y and Yao L 2018 *J. Appl. Phys.* **124** 213901
[10] Yu Z, Zhang G, Qiu Q, Zhang D, Sun X, Wang S, Liu Y, Feng W, Li W and Ai L 2019 *J. Supercond. Nov. Magn.* **32** 1605
[11] Yang Y and Wu Y 2020 *J. Appl. Phys.* **128** 053905
[12] Huang C, Xu B and Zhou Y 2020 *J. Appl. Phys.* **127** 193907
[13] Antončík F, Lojka M, Hlásek T, Bartůněk V, Valiente-Blanco I, Perez-Diaz J L and Jankovský O 2020 *Supercond. Sci. Technol.* **33** 045010
[14] Shi D, Qu D, Sagar S and Lahiri K 1997 *Appl. Phys. Lett.* **70** 3606
[15] Tent B A, Qu D and Shi D 1998 *Physica C* **309** 89
[16] Yang W, Zhou L, Feng Y, Zhang P, Chen S, Wu M, Zhang C, Wang J, Du Z, Wang F, Yu Z, Wu X, Gawalek W and Gorner P 1998 *Physica C* **307** 271
[17] Yang W, Feng Y, Zhou L, Zhang P, Wu M, Chen S, Wu X and Gawalek W 1999 *Physica C* **319** 164
[18] Zhao B, Deng Z, Hu Z, Liu Y, Zhang S and Zheng J 2020 *IEEE Trans. Appl. Supercond.* **30** 6800305
[19] Ruiz-Alonso D, Coombs T A and Campbell A M 2005 *Supercond. Sci. Technol.* **18** S209
[20] Gou X, Zheng X and Zhou Y 2007 *IEEE Trans. Appl. Supercond.* **17** 3795
[21] Zheng X and Yang Y 2007 *IEEE Trans. Appl. Supercond.* **17** 3862
[22] Ma G, Wang J and Wang S 2010 *IEEE Trans. Appl. Supercond.* **20** 2219
[23] Navau C, Del-Valle N and Sanchez A 2013 *IEEE Trans. Appl. Supercond.* **23** 8201023
[24] Badía-Majós A, Aliaga A, Letosa-Fleta J, Alfonso M M and Roche J P 2015 *IEEE Trans. Appl. Supercond.* **25** 3601810
[25] Sass F, Dias D H N, Sotelo G G and de Andrade Junior R 2018 *Supercond. Sci. Technol.* **31** 025006
[26] Navau C and Sanchez A 2001 *Phys. Rev. B* **64** 214507
[27] Valle N D, Sanchez A, Pardo E, Chen D X and Navau C 2007 *Appl. Phys. Lett.* **90** 042503
[28] Bernstein P, Noudem J and Dupont L 2016 *Supercond. Sci. Technol.* **29** 075007
[29] Bernstein P, Colson L, Dupont L and Noudem J 2017 *Supercond. Sci. Technol.* **30** 065007
[30] Davis L C, Logothetis E M and Soltis R E 1988 *J. Appl. Phys.* **64** 4212
[31] Alqadi M K 2015 *Chin. Phys. B* **24** 118404
[32] Kordyuk A A 1998 *J. Appl. Phys.* **83** 610
[33] Hull J R and Cansiz A 1999 *J. Appl. Phys.* **86** 6396
[34] Yang Y and Zheng X 2007 *J. Appl. Phys.* **101** 113922
[35] Zhang X, Zhou Y and Zhou J 2008 *Physica C* **468** 401
[36] Wu X, Xu K, Cao Y, Hu S, Zuo P and Li G 2013 *Physica C* **486** 17
[37] Cansiza A, Yildizerb İ and McGuiness D T 2019 *Cryogenics* **98** 60
[38] Bernstein P and Noudem J 2020 *Supercond. Sci. Technol.* **33** 033001
[39] Alzoubi F Y, Al-khateeb H M, Alqadi M K and Ayoub N Y 2005 *Supercond. Sci. Technol.* **18** 1329
[40] Coffey M W 2000 *Journal of Superconductivity* **13** 381
[41] Coffey M W 2002 *Journal of Superconductivity* **15** 257
[42] Alqadi M K, Alzoubi F Y and Al-khateeb H M 2006 *Mod. Phys. Lett. B* **20** 1549
[43] Al-khateeb H M, Alqadi M K, Alzoubi F Y and Ayoub N Y 2007 *Chin. Phys. Lett.* **24** 2700
[44] Palaniappan D 2009 *J. Supercond. Nov. Magn.* **22** 471
[45] Diez-Jimenez E, Valiente-Blanco I and Perez-Diaz J 2013 *J. Supercond. Nov. Magn.* **26** 71
[46] Alqadi M K, Alzoubi F Y, Al-khateeb H M and Ayoub N Y 2009 *Physica B* **404** 1781
[47] Sivrioglu S and Cinar Y 2007 *Supercond. Sci. Technol.* **20** 559
[48] Sivrioglu S and Basaran S 2015 *IEEE Trans. Appl. Supercond.* **25** 3601507
[49] Basaran S and Sivrioglu S 2017 *Supercond. Sci. Technol.* **30** 035008